1   Reply to comments, Referee #1

2   We would like to thank Referee #1 for his/her time, constructive and helpful comments, edits and suggestions.

3
4   **L42: 'give a MRD of -32.4 ± (56.3) %, . . .These results indicate that the IASI-NH3 product performs**
5   **better than previous upper bound estimates (-50% - +100%).'**
6   **Really better? But -32.4%-56.3% < -50%.**
7   The sentence did not entirely reflect the meaning. Former estimates were made on an expert guess basis/
8   comparison with ground observations. The new estimate is the first which is fully based on column
9   measurements and a better estimate of the performance of the product.

10
11 Line 42 changed to:
12 These results give an improved estimate of the IASI-NH$_3$ product performance compared to the previous upper
13 bound estimates (-50% - +100%).

14
15
16 **L160: 'We excluded stations which have only retrieved or are believed to have, NH3 total columns**
17 **smaller than. . .' However, those cases are also interesting to check for any overestimation of NH3**
18 **columns in the IASI dataset (many of the enhancements seen in Figure 1 in remote areas might be**
19 **artefacts.)**

20
21 We agree on this with the reviewer. However because of time restriction we chose to focus on this set of
22 stations. Also we excluded high altitude stations located in regions with large variations of altitude, i.e.
23 Jungfraujoch/Maido. The remaining possible stations/sites are mostly located in the arctic or Antarctic regions
24 and not of direct interest to this study. All observations shown in Figure 1 were used as input in the comparison.

25
26 **L246: 'To account for the topography we only used observations which have at maximum an altitude**
27 **difference of 300 m between the location of the FTIR and the IASI pixel position.'**
28 **But this criterion does not allow to exclude all cases where there is a mountain between FTIR and IASI**
29 **measurement but still FTIR and IASI are at the same altitude. It should be extended also to the 'way'**
30 **between FTIR and IASI position. Can you exclude such a case?**

31
32 This is already the case, changed line 246 to:
33 To account for the topography we only used observations which have at maximum an altitude difference of 300
34 m (in) between the location of the FTIR and the IASI pixel position.

35
36 **L253:**
37 **Please give the information whether the temporal criterion restricts the comparison dataset to the cases of**
38 **daytime IASI measurements.**

39
40 Only daytime measurements were used in this study, nighttime observations can be compared but the number of
41 coinciding observations is very low due to the small number of nighttime observations (only during summers is
42 the sun still high enough during the late evening ~local time 21.30). See line nr 128, where it was mentioned
43 that we use the morning overpasses only.

44
45 **L275:**
46 **Please specify the source of the skin temperature together with its uncertainty.**
47 Source is the IASI L2 temperature profiles,

48
49 Added Line 276:
50 The Tskin temperatures are obtained from the IASI L2 temperature profiles which have an uncertainty of ~2 K
51 at the surface (August et al., 2012).

52
53 Added reference:
54 August, T., Klaes, D., Schlüssel, P., Hultberg, T., Crapeau, M., Arriaga, A., O'Carroll, A., Coppens, D., Munro,
55 R. and Calbet, X.: IASI on Metop-A: Operational Level 2 retrievals after five years in orbit, J. Quant. Spectrosc.
56 Radiat. Transf., 113(11), 1340–1371, doi:10.1016/j.jqsrt.2012.02.028, 2012.

57
58 **L300:**

To apply this method seems a bit strange since the satellite profile retrieval is not vertically resolved at all, but the FTIRs are. One should test how much the results change in case this method is not applied. Further, it should be possible to calculate a typical averaging kernel of the IASI retrievals by theoretical simulations.

The effects are minor for most sites except for the stations with a large number of the IASI "sea" profile retrieved observations, i.e. for Wollongong and St. Denis.

Typical averaging kernel; a typical averaging could be calculated, but the discussion remains to be about what is to be "typical". Something more applicable would be multiple "typical" AVK cases depending on terrain/climate classes. Either way this would introduce more uncertainty instead of dealing/solving the current ones.

L407: 'successful comparison' It is not clear what 'successful' should mean here. Try to be more specific.

Removed the word "successful"

L462ff.: possible explanation for the negative bias of satellite data. Don't one expect an underestimation of total columns from satellite mid-IR observations especially for gases with maxima very near to the surface due to the small thermal contrast there? The FTIR instruments, however, observe the entire columns. This difference would be included in case correct satellite averaging kernels could be used. This should be discussed more in detail.

This is true, however the exact effect cannot be estimated due to the variability of the sensitivity from observation to observation. A short section has been added to the discussion; from Line 491 onward:

Fourth, the negative bias of the satellite observations can be expected by the lack of sensitivity to concentrations near the surface. This is of course where the ammonia concentrations usually peak. The FTIR observations however do fully observe the lower layers in the troposphere thus causing a discrepancy. Normally one can correct for this using the averaging kernel of the satellite observations. However, the IASI-NH$_3$ retrieval does not produce an averaging kernel meaning it is not possible to calculate the exact effect. The use of a typical averaging kernel will cause more uncertainty as there is a large day to day variability in the averaging kernels as earlier retrievals showed (Clarisse et al., 2009).

Fig. 6 and general:
Both datasets, FTIR and satellite ones, seem to exclude negative values. Is this correct? If yes, how is it achieved (log-retrieval?) and should this not have an effect on the comparison for low column amounts?

The IASI-NH3 retrieval does not retrieve negative total columns following the current retrieval procedure. In case of the FTIR retrieval it is possible to get negative values but due to the retrieval restrictions/settings/procedure it is uncommon. For the "per" station comparison a selection was made, as described in the manuscript, to only use the positive values, in principle this indeed effects the comparison for low column amounts and something like an outlier trim function would be more valid.

Figure 5. Shifted the x- and y- limits to better show the negative values
Figure 6. Added greyed values to show the selected and not selected values.

Technical:
L30-32:
the term 'observations' appears 4 times, try to reformulate
Changed Line 30-32;
Line 30: daily observations to (bi-) daily overpasses.
Line 31: surface observations to surface measurements.

L180 and throughout the manuscript: '60km' -> '60 km' blank between unit and number
Added a blank space to " km " in lines: L151, L182,L185, L359, L498, table 2, caption figure 3, figure 4, figure 5, figure 6 and figure A1.
Table 1 caption: 'The topography described the typography of the region' Please correct.
Changed part of Table 1 caption to: The topography describes the geography of the region surrounding the site.

115   Reply to comments, Referee #2

116   We would like to thank Referee #2 for his/her time, constructive and helpful comments, edits and suggestions.
117
118   **One overall point that should be stated clearly is that the IASI observation sensitivity is not taken into**
119   **consideration in these comparisons given the IASI retrieval approach, which limits the information**
120   **available to explain the differences seen between the IASI and the FTIR.**
121   This point was already shortly mentioned in section 2.3.2. We've added a section in the discussion following a
122   comment of Referee nr 1. In addition, we would like to point out that the IASI retrieval product does come with
123   uncertainty estimates which characterize IASI's sensitivity. These depend on the thermal contrast and total
124   column of NH3. We decided to use a filter for on TC, which captures the main sensitivity component to prevent
125   introducing any biases.
126
127
128   **1) Section 2.3.1: This section talks about the important spatial and temporal differences between the**
129   **FTIR and IASI, which is very well done. However, due to the IASI retrieval approach the sometimes**
130   **equally important vertical sampling difference are not taken into consideration. One sentence should be**
131   **added stating that this difference cannot be determined due to the IASI retrieval and is thus ignored in**
132   **this comparison.**
133
134   Line added to the end of the section: Vertical sampling differences are not taken into consideration in this study
135   however the IASI selection criterion on the thermal contrast is conservative and only those measurements for
136   which IASI has a good sensitivity to surface concentrations are selected.
137
138   **2) Line 246 change the "which" to a "that".**
139
140   Changed as suggested.
141
142   **3) Section 2.3.2 lines 292-292: In might be more clear to the reader if the following was**
143   **added to the end of the sentence,"The effect of the lack of the satellite averaging kernel**
144   **is hard to predict so the satellite vertical sensitivity is not taken into consideration in this**
145   **comparison.**
146
147   We have added: "… so the satellite vertical sensitivity is only taken into account through the selection criterion
148   on the thermal contrast."
149
150   **4) Also, in this section the authors provided a good response in regards to explaining where the x_sat**
151   **IASI profiles are coming from, however, this information was not explicitly added to the text. It would be**
152   **good to add in some the response provided:**
153   **The IASI profiles are not fully retrieved profiles but the fixed shape profiles used as an assumption in the**
154   **IASI retrieval, see Van Damme et al., 2015. These fixed profiles are used for scaling purposes to be able to**
155   **account for the FTIR averaging kernel. Van Damme, M., Clarisse, L., Dammers, E., Liu, X., Nowak, J.**
156   **B., Clerbaux, C., Flechard, C. R., Galy-Lacaux, C., Xu, W., Neuman, J. A., Tang, Y. S., Sutton, M. A.,**
157   **Erisman, J. W., and Coheur, P. F.: Towards validation of ammonia (NH3) measurements from the IASI**
158   **satellite, Atmos. Meas. Tech., 8, 1575-1591, doi:10.5194/amt-8-1575-2015, 2015.**
159   Sentence was added to line 296,
160   The IASI profiles are not fully retrieved profiles but fixed shape profiles used as an assumption in the IASI
161   retrieval, see Van Damme et al., 2015a. These fixed profiles are used for scaling purposes to be able to account
162   for the FTIR averaging kernel.
163
164   **5) It would be nice to added in the rationale for why total column averaging kernels were not used as**
165   **discussed in your response. Just a simple statement acknowledging that total column AK could be used,**
166   **but this should in principle be the same as the procedure used here . . ..**
167   Line 297; added: A total column averaging kernel could be used instead, but in principle is similar to the
168   procedure described here.
169
170   **6) Line 509: the reference "Shepherd" should be "Shephard" to match the reference list.**
171   Changed Shepherd to Shephard.
172

173

An evaluation of IASI-NH$_3$ with ground-based FTIR measurements

Enrico Dammers[1], Mathias Palm[2], Martin Van Damme[1,3], Corinne Vigouroux[4], Dan Smale[5], Stephanie Conway[6], Geoffrey C. Toon[7], Nicholas Jones[8], Eric Nussbaumer[9], Thorsten Warneke[2], Christof Petri[2], Lieven Clarisse[3], Cathy Clerbaux[3], Christian Hermans[4], Erik Lutsch[6], Kim Strong[6], James W. Hannigan[9], Hideaki Nakajima[10], Isamu Morino[11], Beatriz Herrera[12], Wolfgang Stremme[12], Michel Grutter[12], Martijn Schaap[13], Roy J. Wichink Kruit[14], Justus Notholt[2], Pierre.-F. Coheur[3] and Jan Willem Erisman[1,15]

1. Cluster Earth and Climate, Department of Earth Sciences, Vrije Universiteit Amsterdam, Amsterdam, the Netherlands
2. Institut für Umweltphysik, University of Bremen, Bremen, Germany
3. Spectroscopie de l'Atmosphère, Service de Chimie Quantique et Photophysique, Université Libre de Bruxelles (ULB), Brussels, Belgium
4. Royal Belgian Institute for Space Aeronomy (BIRA-IASB), Brussels, Belgium
5. National Institute of Water and Atmosphere, Lauder, New Zealand
6. University of Toronto, Toronto, Ontario, Canada
7. Jet Propulsion Laboratory, California Institute of Technology, Pasadena
8. University of Wollongong, Wollongong, Australia
9. NCAR, Boulder, Colorado, United States
10. Atmospheric Environment Division, National Institute for Environmental Studies (NIES), Japan
11. National Institute for Environmental Studies, 16-2 Onogawa, Tsukuba, Ibaraki, 305-8506, Japan
12. Centro de Ciencias de la Atmosfera, Universidad Nacional Autonoma de Mexico, Mexico City, Mexico
13. TNO Built Environment and Geosciences, Department of Air Quality and Climate, Utrecht, the Netherlands
14. National Institute for Public Health and the Environment (RIVM), Bilthoven, the Netherlands
15. Louis Bolk Institute, Driebergen, the Netherlands

Correspondence to: E. Dammers (e.dammers@vu.nl)

Abstract. Global distributions of atmospheric ammonia (NH$_3$) measured with satellite instruments such as the Infrared Atmospheric Sounding Interferometer (IASI) contain valuable information on NH$_3$ concentrations and variability in regions not yet covered by ground based instruments. Due to their large spatial coverage and (bi-) daily ~~observations~~overpasses, the satellite observations have the potential to increase our knowledge of the distribution of NH$_3$ emissions, and associated seasonal cycles. However the observations remain poorly validated, with only a handful of available studies often using only surface ~~observations~~ measurements without any vertical information. In this study, we present the first validation of the IASI-NH$_3$ product using ground-based Fourier Transform InfraRed (FTIR) observations. Using a recently developed consistent retrieval strategy, NH$_3$ concentration profiles have been retrieved using observations from nine Network for the Detection of Atmospheric Composition Change (NDACC) stations around the world between 2008- 2015. We demonstrate the importance of strict spatio-temporal collocation criteria for the comparison. Large differences in the regression results are observed for changing intervals of spatial criteria, mostly due to terrain characteristics and the short lifetime of NH$_3$ in the atmosphere. The seasonal variations of both datasets are consistent for most sites. Correlations are found to be high at sites in areas with considerable NH$_3$ levels, whereas correlations are lower at sites with low atmospheric NH$_3$ levels close to the detection limit of the IASI instrument. A combination of the observations from all sites (N$_{obs}$ = 547) give a MRD of -32.4 ± (56.3) %, a correlation r of 0.8 with a slope of 0.73. These results give an improved estimate of the IASI-NH3 product performance compared to the previous upper bound estimates (-50% - +100%). ~~These results indicate that the IASI-NH$_3$ product performs better than previous upper bound estimates (-50% - +100%).~~

219

6

1. Introduction

Humankind has increased the global emissions of reactive nitrogen to an unprecedented level (Holland et al., 1999; Rockström et al., 2009). The current global emissions of reactive nitrogen are estimated to be a factor four larger than pre-industrial levels (Fowler et al., 2013). Consequently atmospheric deposition of reactive nitrogen to ecosystems has substantially increased as well (Rodhe et al., 2002; Dentener et al., 2006). Ammonia (NH_3) emissions play a major role in this deposition with a total emission of 49.3Tg in 2008 (Emission Database for Global Atmospheric Research (EDGAR), 2011). Although NH_3 emissions are predominantly from agriculture in the Northern Hemisphere, wildfires also play a role, with biomass burning contributing up to 8% of the global emission budget (Sutton et al., 2013). NH_3 has been shown to be a major factor in the acidification and eutrophication of soil and water bodies, which threatens biodiversity in vulnerable ecosystems (Bobbink et al., 2010; Erisman et al., 2008, 2011). Through reactions with sulphuric and nitric acid, NH_3 also contributes to the formation of particulate matter which is associated with adverse health effects (Pope et al., 2009). Particulate ammonium salts contribute largely to aerosol loads over continental regions (Schaap et al., 2004). Through its role in aerosol formation, NH_3 also has an impact on global climate change as hygroscopic ammonium salts are of importance for the aerosol climate effect and thus the global radiance budget (Adams et al., 2001). Furthermore increased NH_3 concentrations in the soil also enhance the emission of nitrous oxide (N_2O) which is an important greenhouse gas and an ozone-depleting substance (Ravishankara et al., 2009). Finally nitrogen availability is a key factor for the fixation of carbon dioxide (CO_2) and thus it is an important factor in climate change.

Despite the fact that NH_3 at its current levels is a major threat to the environment and human health, relatively little is known about its total budget and global distribution (Sutton et al., 2013; Erisman et al., 2007). Surface observations are sparse and mainly available for north-western Europe, the United States and China (Van Damme et al., 2015a). At the available sites, in situ measurements are mostly performed with relatively poor temporal resolution due to the high costs of performing reliable NH_3 measurements with high temporal resolution. These measurements of NH_3 are also hampered by sampling artefacts caused by the reactivity of NH_3 and the evaporation of ammonium nitrate (Slanina et al., 2001; von Bobrutzki et al., 2010; Puchalski et al., 2011). As the lifetime of atmospheric NH_3 is rather short, on the order of hours to a few days, due to efficient deposition and fast conversion to particulate matter, the existing surface measurements are not sufficient to estimate global emissions without inducing large errors. The lack of vertical profile information further hampers the quantification of the budget, with only a few reported airborne measurements (Nowak et al., 2007, 2010, Leen et al., 2013, Whitburn et al., 2015).

Advanced IR-sounders such as the Infrared Atmospheric Sounding Interferometer (IASI), the Tropospheric Emission Spectrometer (TES), and the Cross-track Infrared Sounder (CrIS) enable retrievals of atmospheric NH_3 (Beer et al., 2008; Coheur et al., 2009; Clarisse et al., 2009; Shephard et al., 2011, 2015a). The availability of satellite retrievals provide a means to consistently monitor global NH_3 distributions. Global distributions derived from IASI and TES observations have shown high NH_3 levels in regions not covered by ground-based data. In this way, more insight was gained into known and unknown NH_3 sources worldwide including biomass burning, industry and agricultural areas. Hence, satellite observations have the potential to improve our

7

259 knowledge of the distribution of global emissions and their seasonal variation due to their large spatial coverage
260 and (bi-) daily observations (Zhu et al., 2013; Van Damme et al., 2014b, 2015b; Whitburn et al., 2015; Luo et
261 al., 2015). However, the satellite observations remain poorly validated with only a few dedicated campaigns
262 performed with limited spatial, vertical or temporal coverage (Van Damme et al., 2015a; Shephard et al., 2015b,
263 Sun et al., 2015).

264 Only a few studies have explored the quality of the IASI-NH$_3$ product. A first evaluation of the IASI
265 observations was made over Europe using the LOTOS-EUROS model and has shown the respective consistency
266 of the measurements and simulations (Van Damme et al., 2014b). A first comparison using ground-based and
267 airborne measurements to validate the IASI-NH$_3$ data set were made in Van Damme et al. (2015a). They
268 confirmed consistency between the IASI-NH$_3$ data set and the available ground-based observations and showed
269 promising results for validation by using independent airborne data from the CalNex campaign. Nevertheless,
270 that study was limited by the availability of independent measurements and suffered from representativeness
271 issues for the satellite observations when comparing to surface concentration measurements. One of the key
272 conclusions was the need for vertical profiles (e.g. ground-based remote sensing products or upper-air in situ
273 measurements to compare similar quantities). Recently, Dammers et al. (2015) developed a retrieval
274 methodology for Fourier Transform Infrared Spectroscopy (FTIR) instruments to obtain remotely sensed
275 measurements of NH$_3$ and demonstrated the retrieval characteristics for four sites located in agricultural and
276 remote areas. Here we explore the use of NH$_3$ total columns obtained with ground based FTIR at nine stations
277 with a range of NH$_3$ pollution levels to validate the IASI-NH$_3$ satellite product by Van Damme (2014a).

278 First, we concisely describe the ground based FTIR retrieval and IASI-NH$_3$ product datasets in Sections 2.1 and
279 2.2. Next we describe the methodology of the comparison in Section 2.3 followed by the presentation of the
280 results in Section 3, which are then summarized and discussed in Section 4.

281

2. Description of the satellite and FTIR data sets and validation methodology

2.1 IASI-NH$_3$ product

The first global NH$_3$ distribution was obtained by a conventional retrieval method applied to IASI spectra (Clarisse et al., 2009), followed by an in depth case study, using a more sophisticated algorithm, of the sounder's capabilities depending on the thermal contrast (defined in Van Damme et al. (2014a) as the temperature differences between the Earth surface and the atmosphere at 1.5 km altitude, Clarisse et al., 2010). In this study we use the NH$_3$ product developed by Van Damme et al. (2014a). Their product is based on the calculation of a dimensionless spectral index (Hyperspectral Range Index: HRI), which is a quantity representative of the amount of NH$_3$ in the total atmospheric column. This HRI is then converted into NH$_3$ total columns using look-up-tables based on numerous forward simulations for various atmospheric conditions. These look-up-tables relate the HRI and the thermal contrast to a total column of NH$_3$ (Van Damme et al., 2014a). The product includes an error characterization of the retrieved column based on errors in the thermal contrast and HRI. Important advantages of this method over the method by Clarisse (2009) is the relatively small computational cost, the improved detection limit and the ability to identify smaller emission sources and transport patterns above the sea. One of the limitations of this method is the use of only two NH$_3$ vertical profiles: a "source profile" for land cases and a "transported profile" for sea cases (Illustrated in Van Damme et al., 2014a, fig. 3). Another limitation of the product is that it does not allow the calculation of an averaging kernel to account for the vertical sensitivity of the instrument sounding to different layers in the atmosphere. In this paper we will use NH$_3$ total columns retrieved from the IASI-A instrument (aboard of the MetOp-A platform) morning overpass (AM) observations (i.e. 09:30 local time at the equator during overpass) which have a circular footprint of 12 km diameter at nadir and an ellipsoid shaped footprint of up to 20 km x 39 km at the outermost angles. We will use observations from January 1st 2008 to December 31st 2014. Figure 1 shows the mean IASI-NH$_3$ total column distribution (all observations gridded to a 0.1° x 0.1° grid) using observations above land for the years 2008-2014. The mean columns are obtained through a weighting with the relative error (see Van Damme et al., 2014). The bottom left inset shows the corresponding relative error.

2.2 FTIR- NH$_3$ retrieval

The FTIR-NH$_3$ retrieval methodology used here is described in detail in Dammers et al. (2015) and a summary is given here. The retrieval is based on the use of two spectral micro-windows, which contain strong individual NH$_3$ absorption lines. The two spectral windows [930.32-931.32 cm^{-1}, MW1] and [962.70-970.00 cm^{-1}, MW2] or the wider version for regions with very low concentrations [929.40-931.40 cm^{-1}, MW1 Wide] and [962.10-970.00 cm^{-1}, MW2 Wide] are fitted using SFIT4 (Pougatchev et al., 1995; Hase et al., 2004, 2006) or a similar retrieval algorithm (Hase et al, 1999) based on the optimal estimation method (Rodgers et al., 2000) to retrieve the volume mixing ratios (in ppbv) and total columns of NH$_3$ (in molecules cm^{-2}). Major interfering species in these windows include H$_2$O, CO$_2$ and O$_3$. Minor interfering species are N$_2$O, HNO$_3$, CFC-12 and SF$_6$. For the line spectroscopy, the HITRAN 2012 (Rothman et al., 2013) database is used with a few adjustments for CO$_2$ (ATMOS, Brown et al., 1996), and sets of pseudo-lines generated by NASA-JPL (G.C. Toon) are used for the broad absorptions by heavy molecules (i.e. CFC-12, SF$_6$). The *a-priori* profiles of NH$_3$ are based on balloon measurements (Toon et al., 1999) and scaled to fit common surface concentrations at each of the sites. An exception is made for the a-priori profile at Reunion Island where a modelled profile from the MOZART model is used (Louisa Emmons, personal communication, 2014). There, the profile peaks at a height of 4-5 km, as NH$_3$ are expected to be due to transport of biomass burning emissions on the island and Madagascar. For all stations, the *a-priori* profiles for interfering species are taken from the Whole Atmosphere Community Climate Model (WACCM, Chang et al., 2008). Errors in the retrieval are typically ~30% (Dammers et al., 2015), which are mostly due to uncertainties in the spectroscopy in the line intensities of NH$_3$ and the temperature and pressure broadening coefficients (HITRAN 2012).

An effort has been made to gather observations from most of the station part of the Network for the Detection of Atmospheric Composition Change (NDACC) which have obtained relevant solar spectra between 1st of Jan 2008 and 31st of Dec 2014. We excluded stations which have only retrieved or are believed to have, NH$_3$ total columns smaller than 5x10^{15} (molecules cm^{-2}) during the study interval (i.e. Arctic and Antarctic and other stations with concentrations below the expected limits of the IASI-NH$_3$ product, at best ~5x10^{15} for observations with high thermal contrast). Figure 1 shows the positions of the FTIR stations used in this study. The retrieved NH$_3$ total columns (molecules cm^{-2}) for each of the stations are shown in Figure 2. The number of available observations per station varies as does the range in total columns with high values of ~100x10^{15} (molecules cm^{-2}) observed at Bremen and low values of about 1x10^{15} (molecules cm^{-2}) at St Denis Reunion. The following provides a short description of each of the sites used in this study and retrieved NH$_3$ columns (molecules cm^{-2}). Additionally, a short summary can be found in Table 1:

The **Bremen** site operated on the university campus by the University of Bremen in the northern part of the city (Velazco et al., 2007). Bremen is located in the northwest of Germany, which is characterized by intensive agriculture. It is most suitable for comparisons with IASI given the very high observed concentrations (Fig. 2, blue) and flat geography surrounding the station. NH$_3$ sources near the measurement station include manure application to fields, livestock housing and exhaust emissions of local traffic. The retrieved NH$_3$ total columns peak in spring due to manure application and show an increase in summer due to increased volatilization of NH$_3$ from livestock housing and fields when temperatures increase during summer.

10

349 The **Toronto** site (Wiacek et al., 2007) is located on the campus of the University of Toronto, Canada. The city

350 is next to Lake Ontario with few sources to the south. NH_3 sources are mainly due to agriculture as well as local

351 traffic in the city. Occasionally, NH_3 in smoke plumes from major boreal fires to the north and west of the city

352 can be observed (Lutsch et al., 2016). The retrieved columns (Fig. 2, green) show increased values during

353 summers as well as peaks in spring.

354 The **Boulder** observation site is located at the NCAR Foothills Lab in Boulder, Colorado, United States of

355 America, about 60 km northwest of the large metropolitan Denver area. It is located at 1.6 km a.s.l. on the

356 generally dry Colorado Plateau. Directly to the west are the foothills of the Rocky Mountain range and to the

357 east are rural grasslands, farming and ranching facilities. Among them are large cattle feed lots to the northeast

358 near Greeley approximately 90 km distant. The area is subject to occasional seasonal local forest fires and also

359 occasionally sees plumes from fires as distant as Washington or California. The retrieved columns (Fig. 2, grey)

360 show the largest increase during summers.

361 The **Tsukuba** site (Ohyama et al., 2009) is located at the National Institute for Environmental Studies (NIES),

362 in Japan. The region is a mixture of residential and rural zones with mountains to the north. NH_3 sources near

363 the measurement site include manure and fertilizer applications and exhaust emissions of local traffic in the

364 surrounding city with a large part originating from the from the Tokyo metropolitan area. The retrieved columns

365 (Fig 2, red) show a general increase during the summers due to increased volatilization rates.

366 The **Pasadena** site lies on the Northern edge of the Los Angeles conurbation in the United States of America, at

367 the foot of the San Gabriel mountains which rise steeply to the north to over 1.5 km altitude within 5 km

368 distance. Local sources of NH_3 include traffic, livestock, and occasional fires. FTIR observations typically take

369 place around local noon to avoid solar obstruction by nearby buildings and morning stratus cloud that is

370 common May-July. The highest retrieved columns (Fig.2, cyan) are observed during the summers.

371 The **Mexico City** site is located on the campus of the National Autonomous University of Mexico (UNAM) at

372 2280 m a.s.l., south of the metropolitan area. Surface NH_3 concentrations were measured by active open-path

373 FTIR during 2003 with typical values between 10 - 40 ppb (Moya et al. 2004). The megacity is host to more

374 than 22 million inhabitants, over 5 million motor vehicles and a wide variety of industrial activities. Low

375 ventilation during night and morning causes an effective accumulation of the NH_3 and other pollutants in

376 Mexico City, which is located in a flat basin surrounded by mountains. The concentration and vertical

377 distribution of pollutants are dominated by the large emissions and the dynamics of the boundary layer which is

378 on average 1.5 km height during the IASI morning overpass (Stremme et al., 2009, 2013). The retrieved

379 columns (Fig.2, orange) show an increase during the summers as well as a large daily variation.

380 The measurement site on the university campus of **St.-Denis** (Senten et al., 2008) is located on the remote

381 Reunion Island in the Indian Ocean. Observed NH_3 columns (Fig. 2, purple) are usually low due to the lack of

382 major sources nearby the site but increases are observed during the fire season (Sept.-Nov.) with possible fire

383 plumes originating from Madagascar, as already observed in another study involving short-lived species

384 (Vigouroux et al., 2009). Local NH_3 emissions include fertilizer applied for sugar cane production and local

385 biomass burning.

386 The **Wollongong** site is located on the campus of the University of Wollongong. The city of Wollongong is on

387 the south east coast of Australia with the University only about 2.5 km from the ocean. The measurement site is

388 also influenced by a 400m escarpment 1 km to the West, and the city of Sydney 60 km to the north. NH_3

389 sources come mainly from city traffic, as well as seasonal forest fires that can produce locally high amounts of
390 smoke and subsequent NH$_3$ emissions (Paton-Walsh et al., 2005). The retrieved columns (Fig.2, brown) peak
391 during the summer season due to the higher temperatures and seasonal forest fires.
392 The **Lauder** (Morgenstern et al., 2012) National Institute of Water and Atmospheric Research (NIWA) station
393 in Central Otago, New Zealand, is located in a hilly region with NH$_3$ emissions in the valley surrounding the
394 station mostly due to livestock grazing and fertilizer application. The observed columns (Fig. 2, black) show a
395 general increase during summers due to increased volatilization rates.
396
397

2.3 FTIR and satellite comparison methodology
2.3.1 Co-location & data criteria

NH$_3$ is highly variable in time and space which complicates the comparison between the IASI and FTIR observations. Therefore collocation criteria were developed to investigate and mitigate the effect of the spatial and temporal differences between the FTIR and IASI observations on their correlation. So far, there is no model to describe the representativeness of a site for the region so a simple criterion was initially derived by analyzing the terrain around each site and comparing the correlation of the IASI and FTIR observations for multiple time and spatial differences to find the best correlation. To illustrate the differences between the representativeness of the sites we take the stations at Bremen, Lauder and Wollongong as examples. Around Bremen the terrain is flat with high reported NH$_3$ emissions (Kuenen et al., 2014) in the region surrounding the city. In contrast, Lauder is located in a hilly region with low NH$_3$ emissions mostly due to local livestock grazing and fertilizer application in the surrounding valleys (EDGAR, 2011). Owing to the flat terrain, the region around Bremen should, in principle, have more homogeneous concentrations than Lauder. A more extreme case for geographical inhomogeneity is Wollongong. Wollongong is located at the coast near a 400m escarpment without major nearby NH$_3$ sources. Hence increasing distances between the satellite measurement pixel center and the station may negatively impact the comparison due to the short lifetime of NH$_3$, and the limitation on transport of NH$_3$ to the site by the terrain (i.e. representativeness problems). Because no uniform criterion was found that would enable a good comparison for all stations, multiple criteria with a maximum difference of between 10 km and 50 km will be used to analyze the optimal setting for each of the sites. Vertical sampling differences are not taken into consideration in this study however the IASI selection criterion on the thermal contrast is conservative and only those measurements for which IASI has a good sensitivity to surface concentrations are selected.

Topography

Any hill or mountain range located between the satellite pixel and the FTIR station may inhibit transport and decrease their comparability. To account for the topography we only used observations which that have at maximum an altitude difference of 300 m (in) between the location of the FTIR and the IASI pixel position. The 300 m criterion was chosen based on tests using the FTIR and satellite observations from Lauder. For the calculation of the height differences we used the Space Shuttle Radar Topography Mission Global product at 3 arc second resolution (SRTMGL3, Farr et al., 2007).

Temporal variation

NH$_3$ concentrations can vary considerably during the day, with lifetimes as short as a few hours not being uncommon (Dentener and Crutzen, 1994; Bleeker et al., 2009). The variability of the concentrations mainly arises from the variability in emission strengths as influenced by agricultural practices, meteorological, and atmospheric conditions such as temperature, precipitation, wind speed and direction, the development of the boundary layer (which is important as the IASI satellite observations take place around 9.30 local time and thus the boundary layer has not always been fully established), pollution level, and deposition rates. To minimize the effects of this variability on the comparability of the IASI and FTIR observations, satellite observations with a time difference to FTIR observation of no more than 90 minutes were used.

13

Product error

The error of the IASI-NH$_3$ columns derives from errors on the HRI and the thermal contrast (Van Damme et al., 2014a). Applying relative error filters of 50, 75 and 100% showed that mostly lower concentrations are removed from the comparison. Consequently, introducing any criteria based on the associated (relative) error will bias any comparison with FTIR columns towards the higher IASI total columns. Therefore, we decided not to filter based on the relative error as it skews the range of NH$_3$ column totals.

Meteorological factors

The lowest detectable total column of the retrieval depends on the thermal contrast of the atmosphere (Van Damme et al., 2014a). For example, the retrieval has a minimum detectable NH$_3$ column of around 5×10^{15} molecules cm^{-2} at a thermal contrast of about 12 Kelvin (K) for columns using the "transported" profile. A thermal contrast of 12 K is chosen as the threshold to ensure the quality of the IASI observations, which represents a lapse rate of around 8K/km altitude, near standard atmospheric conditions. We excluded data for T_{skin} temperatures below 275.15 K to introduce a basic filter for snow cover and conditions with frozen soils. The T_{skin} temperatures are obtained from the IASI L2 temperature profiles which have an uncertainty of ~2 K at the surface (August et al., 2012). Finally, only IASI observations with a cloud cover below 10% are used.

The complete list of selection criteria is summarized in Table 2.

Quality of the FTIR observations

No filters were applied to maximize the number of observations usable in the comparison. The resolution and detection limit of the FTIR instruments is usually better than that of the IASI instrument, leading to retrieved columns with, in principle, less uncertainty. Overall the FTIR retrievals show an error of ~30% or less with the largest errors due to the spectroscopic parameters (Dammers et al., 2015). While artefacts are possible in the data we did not investigate for specific artefacts and possible impacts.

2.3.2   Application of averaging kernels

When performing a direct comparison between two remote sensing retrievals, one should take into account the vertical sensitivity and the influence of a-priori profiles of both methods. One method to remove the influence of the a-priori profile and the vertical sensitivity is the application of the averaging kernels of both retrievals to the retrieved profiles of both products. The IASI-NH$_3$ HRI-based product scheme however, does not produce averaging kernels thus it is not possible to account for the vertical sensitivity of the satellite retrieval. The effect of the lack of the satellite averaging kernel is hard to predict, so the satellite vertical sensitivity is only taken into account through the selection criterion on the thermal contrast. Nonetheless following the method described in Rodgers and Connor (2003), the FTIR averaging kernel A is applied to the IASI profile x_{sat} to account for the effects of the a-priori information and vertical sensitivity of the FTIR retrieval (the assumed profiles, called "land" and "sea" are described in Van Damme et al., 2014a). The IASI profiles are not fully retrieved profiles but fixed shape profiles used as an assumption in the IASI retrieval, see Van Damme et al., 2015a. These fixed profiles are used for scaling purposes to be able to account for the FTIR averaging kernel. A total column

14

479 averaging kernel could be used instead, but in principle is similar to the procedure described here. The IASI

480 profile is first mapped to the altitude grid of the FTIR profile by using interpolation, forming x_{sat}^{mapped}. Applying

481 Eqn. (1), the smoothed IASI profile $\hat{x}_{sat}$ is calculated indicating what the FTIR would retrieve when observing

482 the satellite profile, which is then used to compute a total column. This profile can then be compared with the

483 FTIR profile.

484 $$\hat{x}_{sat} = x_{ftir}^{apriori} + A(x_{sat}^{mapped} - x_{ftir}^{apriori}) \qquad\qquad (1)$$

485 After the application of the averaging kernel, for each FTIR observation, all satellite observations meeting the

486 coincident criteria are averaged into a single mean total column value to be compared with the FTIR value. If

487 multiple FTIR observations match a single satellite overpass, taking into account the maximum time difference,

488 the FTIR observations are also averaged into a single mean total column value.

489

490 **3. Results**

491 **3.1 The influence of spatial differences between observations**

492

493 Following the approach of Irie et al. (2012) we will first show the correlation r, the slope as well as the mean

494 relative difference (MRD) and the mean absolute difference (MAD) between satellite (y-axis) and FTIR NH_3

495 total columns (x-axis) for each of the sites, as a function of the maximum allowable spatial difference between

496 the observations (xdiff). The relative difference (RD) is defined here as,

497

498 $$RD = \frac{(IASI\ column - FTIR\ column)\ x\ 100}{FTIR\ column} \qquad\qquad (2)$$

499

500 A maximum relative difference of 200% was used to remove extreme outliers from the data, typically

501 observations under wintertime conditions. The left side of Figure 3 shows the correlation coefficients (blue

502 lines) and slope (red lines) for a selection of sites as a function of xdiff using a maximum allowed sampling time

503 difference of 90 minutes. The right side of Figure 3 shows the MRD and MAD between the satellite and FTIR

504 observations as a function of xdiff. The numbers on the bottom of each of the subfigures show the number of

505 observations used in the comparison. The values in bold beside the title of each subplot give the mean

506 concentrations of the IASI and FTIR observations. The bars indicate the standard deviation of the slope (left

507 side figures) and the relative and absolute differences (right side figures).

508

509 For most stations an increasing xdiff (Figure 3) means a decreasing correlation (blue lines) and a changing slope

510 (either decreasing or increasing with distance, red lines). This can be explained by the local character and high

511 variation of NH_3 emissions/concentration in combination with the locations of the stations. Moving further away

512 from a source will then generally decrease the relation between the concentration in the air and the emission

513 source. The same is true for satellite observations of the air concentrations, which have a large footprint

514 compared to the local character of a point measurement (FTIR) and the emissions. The steepness of this

515 decrease (or increase) tells us something about the local variation in NH_3 concentrations, which can be large for

15

516 sites near heterogeneous emission sources or in cases with low transport/turbulence and thus overall relatively

517 low mixing.

518

519 Overall the highest correlations are seen at the Bremen site, which can partially be explained by the overall high

520 number of observations with high concentrations (more than 15-20e15 molecules cm^{-2}) which generally favours

521 the correlations. The mean column totals as well as the MRD and MAD do not change much except for the

522 smallest xdiff criteria. The larger changes for observations within 15 km are probably due to the smaller number

523 of observations (which follows from the relatively few IASI observations directly above or near the stations).

524 The results show an underestimation of observed columns by IASI with the "all stations" slopes in between

525 ~0.6-0.8. The stations with a lower mean FTIR column totals, such as Toronto and Boulder (as well as

526 Pasadena, Mexico City, and Lauder shown in the Appendix Figure A1) show lower correlations with most

527 having slopes below one. The correlations decreasing with mean column totals point towards the product

528 detection limits of the IASI-NH$_3$ product. The Toronto site has lower correlation coefficients for the smallest

529 xdiffs, but this seems to be due to the large drop in number of observations for a xdiff of <15 km. For higher

530 xdiff criteria the correlations of the Toronto site shows results similar to Bremen. The observations at Boulder

531 also show large differences when including more observations further away from the station. This can be

532 explained by the land use surrounding the Boulder site. Immediately west of the measurement site is a mountain

533 range which together with our elevation filter leads to rejection of the observations to the west. To the northeast

534 there are some major farming areas surrounding the river banks. Correlations do increase with a decreasing

535 xdiff, suggesting that IASI is able to resolve the large gradients in the NH$_3$ concentrations near the site.

536

537 From the correlation analysis as function of spatial coincidence, we conclude that a xdiff value of 25 km is

538 recommended to make a fair comparison between IASI-NH$_3$ and FTIR. Any criteria smaller than 15 km greatly

539 reduces the number of observations and statistics. xdiff beyond 25 km further decrease the correlations for the

540 combined set. From this point onward a xdiff value of 25 km will be used.

541

542 **3.2 Comparison of FTIR and IASI NH3 data**

543 Observations from multiple years are used to show the coincident seasonal variability of the FTIR and IASI-

544 NH$_3$ products for each of the sites (Figure 4, FTIR: blue, IASI: red). Observations are grouped together into a

545 typical year as there are insufficient collocated observations to show an inter-annual time series. Note the

546 different scales on the y-axis. Similar seasonal cycles are clearly observed in both datasets for most stations.

547 Enhanced concentrations in spring are observed for Bremen and Toronto as well as Boulder due to manure

548 application. Most of the sites show an increase of NH$_3$ during the summer months which is likely due to the

549 increased volatilization of NH$_3$ as an effect of higher temperatures. Fire events that were earlier captured by

550 FTIR at St.-Denis in November, as well as in the IASI data, are not observed in the collocated sets, which is due

551 to a lack of coincident observations. Furthermore, there is a lack of observations in wintertime for most of the

552 stations either due to low thermal contrast or due to overcast conditions. Tsukuba has observations above the

553 detection limit but only one year of infrequent observations which is insufficient to show an entirely clear

554 seasonal cycle. A similar thing can be said for Pasadena where the number of coincident observations are too

555 few to make meaningful conclusions about the seasonal cycle. In conclusion, IASI reflects similar pollution
556 levels and seasonal cycles as deduced from the FTIR observations.

557

558 Figure 5 and 6 show a direct comparison of the FTIR and IASI NH$_3$ total columns for each station as well as a
559 combination of all the observations. Correlations, number of observations and slope are shown in the figures.
560 The MRD and these statistics are also summarized in Table 3. The comparison shows a variety of results. As
561 before, of all 9 stations Bremen shows the best correlation with a coefficient of determination of r = 0.83 and a
562 slope of 0.60. The intercept is not fixed at zero. The stations with overall lower observed totals columns (less
563 than $10x10^{15}$ molecules cm^{-2}) show lower correlations. Stations with intermediate concentrations like Toronto
564 and Boulder show correlations r = ~0.7-0.8. The figure also shows the relatively low number of high
565 observations for both the FTIR and IASI values as a result of the relatively few FTIR observations during
566 events. The few outliers can have a disproportional effect on the slope as most of the lower observations are less
567 accurate due to the detection limits of the instruments. Overall most stations, except St.-Denis and Boulder and
568 Mexico City, indicate an underestimation by IASI of the FTIR columns ranging from 10-50%. The mean
569 relative differences for most stations are negative with most showing values in between -22.5 ± (54.0) % for
570 Bremen down to a -61.3 ± (78.7) % for St.-Denis. The bias shows some dependence on the total columns with
571 the underestimation being higher at stations with high mean total columns and lower at stations with low mean
572 total columns. An exception to this are stations with the lowest mean total columns (i.e. St.-Denis and
573 Wollongong). The differences at St.-Denis might be explained by the fact that most IASI observations are
574 positioned above water due to restrictions for terrain height differences. A similar thing can be said for
575 Wollongong which is situated on the coast with hills directly to the inland. Most observations are on the border
576 of water and land which might introduce errors in the retrieval. The combination of all observations gives a
577 MRD of -32.4 ± (56.3) %.

578

579 **4. Discussion and conclusions**

580

581 Recent satellite products enable the global monitoring of atmospheric concentrations of NH$_3$. Unfortunately, the
582 validation of the satellite products of IASI (Van Damme et al., 2014a), TES (Shephard et al., 2011) and CrIS
583 (Shephard et al., 2015a) is very limited and, so far, only based on sparse in-situ and airborne studies. Dammers et
584 al. (2015) presented FTIR total column measurements of NH$_3$ at several places around the world and demonstrated
585 that these data can provide information about the temporal variation of the column concentrations, which are more
586 suitable for validation than ground-level concentrations. Ground-based remote sensing instruments have a long
587 history for validation of satellite products. FTIR observations are already commonly used for the validation of
588 many satellite products, including carbon monoxide (CO), methane (CH$_4$) and nitrous oxide (N$_2$O) (Wood et al.,
589 2002; Griesfeller et al., 2006; Dils et al., 2006; Kerzenmacher et al., 2012). Furthermore, MAX-DOAS systems
590 are used for the validation of retrievals for reactive gases (e.g. Irie et al., 2012), whereas AERONET is widely
591 used to validate satellite-derived aerosol optical depth (e.g. Schaap et al., 2008). The ~~successful~~ comparison
592 between FTIR and IASI NH$_3$ column reported here can be seen as a first step in the validation of NH$_3$ satellite
593 products.

594

In this study, we collected FTIR measurements from nine locations around the world and followed the retrieval described by Dammers et al. (2015). The resulting datasets were used to quantify the bias and evaluate the seasonal variability in the IASI-NH$_3$ product. Furthermore, we assessed the colocation criteria for the satellite evaluation. Additional selection criteria based on thermal contrast, surface temperature, cloud cover and elevation differences between observations, were applied to ensure the quality of the IASI-NH$_3$ observations. The FTIR averaging kernels were applied to the satellite profiles to account for the vertical sensitivity of the FTIR and the influence of the a-priori profiles.

To optimally compare the satellite product to the FTIR observations it is best to reduce the spatial collocation criterion to the size of the satellite instrument's footprint and allow for a time difference as short as possible. These considerations are to reduce effects of transport, chemistry and boundary layer growth but limit the number of coinciding observations significantly. We have shown that the spatial distance between the IASI observations and the FTIR measurement site is of importance: the larger the distance in space, the lower the correlation. When there is no exact match in the position of both observations the variations in the spatial separation lead to correlation coefficients that can greatly change even when changing the spatial criteria (xdiff) from 10 to 30 km. Reasons for the changes are the local nature of NH$_3$ emissions, the surrounding terrain characteristics and their influence on local transport of NH$_3$. The small values for spatial and temporal coincidence criteria show the importance of NH$_3$ sources near the measurement sites when using these observations for satellite validation. For the validation of the IASI observations, we used a xdiff of less than 25 km, which still showed high correlations while a large number of observations is retained for comparison.

Overall we see a broad consistency between the IASI and FTIR observations. The seasonal variations of both datasets look similar for most stations. Increased column values are observed for both IASI and FTIR during summers as the result of higher temperatures, with some sites showing an increase in concentrations due to manure application and fertilization events in spring (Bremen, Toronto). In general our comparison shows that IASI underestimates the NH$_3$ total columns, except for Wollongong. The Wollongong site has persistent low background columns, i.e. observations with a low HRI, to which IASI is not very sensitive, which results in an overestimation of the observed columns. Overall, correlations range from r ~ 0.8 for stations characterised by higher NH$_3$ column totals (with FTIR columns up to 80e15 molecules cm^{-2}) to low r ~ 0.4-0.5 correlations for stations, which only have a few to no FTIR observations above 5×10^{15} molecules cm^{-2}. Hence, the detection limit or sensitivity of the IASI instrument largely explain the lower correlation values. The combination of all sites (N$_{obs}$ = 547) give a MRD of -32.4 ± (56.3) %, a correlation r of 0.8 with a slope of 0.73.

In comparison to ground-based in situ systems, the FTIR observations have the big advantage to provide coarse vertical profiles, from which a column can be derived, which are more similar to what the satellite measures and therefore more useful for validation. Dedicated NH$_3$ validation datasets are needed that better match the overpass times of satellite instruments like IASI, TES and CrIS. This could be achieved by the addition of NH$_3$ to the NDACC measurement protocols and matching the overpass time of these satellites over these measurement stations by using of the right spectral filters for detecting NH$_3$. Furthermore, the low number of NDACC stations and their locations are not optimal for a dedicated validation of NH$_3$ satellite products.

635 Although these provide a starting point, the small set of stations does not cover the entire range of climate
636 conditions, agricultural source types and emission regimes. Hence, our validation results should be seen as
637 indicative. Additional stations or dedicated field campaigns are needed to improve this situation. New stations
638 should be placed in regions where emissions and geography are homogenous to ensure that stations are
639 representative for the footprints of the satellites. For validation of satellite products using FTIR measurements a
640 monitoring and measurements strategy needs to be developed with a representative mixture of locations in
641 addition to ground level data. The later can cover the spatial variation and different temporal measurements can
642 be used. The use of IASI and FTIR observations to study NH_3 distributions at ground level requires a
643 combination of model calculations and observations (e.g. Erisman et al., 2005a; 2005b). Such techniques are
644 required to provide all the necessary details to describe the high spatial and temporal variations in NH_3.
645

646 The direct comparison of the IASI and FTIR columns is an addition to earlier efforts by Van Damme et al.
647 (2015a) to validate IASI column observations with surface in situ and airborne observations. Our results
648 presented here indicate that the product performs better than the previously upper bound estimate of a factor 2
649 (i.e. -50 to +100%) as reported in Van Damme et al. (2014a). Although we tried to diminish any effect of
650 sampling time and position it cannot be ruled out completely that these impacts the comparison statistics as the
651 number of stations is small. Still the picture arising from the different stations is rather consistent, which hints at
652 other issues that may explain the observed bias. A number of important issues concerning the retrieval
653 techniques may explain the observed difference. First, the HRI based retrieval used for IASI is intrinsically
654 different to the optimal estimation based approach used for the FTIR retrieval. An IASI optimal estimation
655 retrieval for NH_3 called FORLI does exist but is not fully operationally used as it is computationally much
656 slower than the HRI method. Surprisingly a first comparison between the FORLI and HRI based retrieval (see
657 figure 9, Van Damme et al., 2014a) shows ~30% lower retrieved columns by the HRI scheme, which is very
658 close to the systematic difference quantified here. Do note that the results are not be fully comparable as the
659 reported HRI-FORLI comparison was for a limited dataset and no quality selection criteria were applied. We
660 recommend to further explore the use of the optimal estimation based IASI-NH_3 retrieval in comparison to the
661 FTIR observations. Second, the IASI and FTIR retrievals incorporate the same line spectroscopy database
662 (HITRAN 2012; Rothman et al., 2013) which removes a possible error due to different spectroscopy datasets.
663 The spectroscopy is the largest expected cause of error in the FTIR observations with measurement noise being
664 the close second for sites with low concentrations. An improvement to the line parameters (i.e. line intensity,
665 pressure and temperature effects) would greatly benefit both the FTIR and IASI retrievals. Thirdly, the HRI
666 based scheme uses the difference between spectra with and without the spectral signature of NH_3. A plausible
667 cause for error in this scheme is the influence and correlation of interfering species in the same spectral
668 channels. H_2O lines occur near most of the NH_3 spectral lines and interfere with the NH_3 lines at the resolution
669 of the IASI instrument. Humidity levels vary throughout the year with an increase amount of water vapour in
670 summer conditions. The HRI based scheme uses a fixed amount of water vapour and varying amounts of water
671 vapour may interfere with the HRI value attributed fully to the NH_3 columns. As there is a seasonality in the
672 water vapour content of the atmosphere (Wagner et al., 2006), any error attributed to water vapour should show
673 a seasonality in the difference between the IASI and FTIR observations. A seasonality was, however, not visible
674 although it may be that the number of coincident observations was too small to recognize it. This again shows

19

675 the need for dedicated NH_3 validation data (e.a. dedicated FTIR observations). Fourth, the negative bias of the
676 satellite observations can be expected by the lack of sensitivity to concentrations near the surface. This is of
677 course where the ammonia concentrations usually peak. The FTIR observations however do fully observe the
678 lower layers in the troposphere thus causing a discrepancy. Normally one can correct for this using the
679 averaging kernel of the satellite observations. However, the IASI-NH_3 retrieval does not produce an averaging
680 kernel meaning it is not possible to calculate the exact effect. The use of a typical averaging kernel will cause
681 more uncertainty as there is a large day to day variability in the averaging kernels as earlier retrievals showed
682 (Clarisse et al., 2009). Finally, another possible cause of error is the lack of a varying NH_3 profile and the proxy
683 used for thermal contrast to describe the state of the atmosphere. The sensitivity of the scheme to the
684 concentrations of NH_3 in the boundary layer is described by using a fixed profile for land and sea observations
685 in combination with a thermal contrast based on two layers (surface and 1.5 km) as it is expected that most of
686 the NH_3 occurs in the boundary layer. In reality the NH_3 profile is highly dynamic due to a varying boundary
687 layer height and changing emissions as well as temperature changes (e.g. inversions etc) occurring throughout
688 the planetary boundary layer. Not accounting for this can introduce an error and future HRI based schemes
689 should focus on estimating the possible effects of using only a specific profile. The use of multiple NH_3-profiles
690 in combination with multiple temperature layers would be a better approximation of state of the atmosphere,
691 although computationally more expensive. The sharp difference between the sea and land retrieval introduces
692 strong variability in observations near the coast. Furthermore, observations that are directly on the transition
693 between water and land can introduce problems due to the varying emissivity. Similar issues have been reported
694 for aerosol retrievals (e.g. Schaap et al., 2008).

695

696 Although the FTIR observations offer some vertical information, studies combining this technique with tower or
697 airborne observations are needed to further improve knowledge and sensitivity of the FTIR and satellite
698 observations to the vertical distribution of NH_3. Without this knowledge, it is not possible to use the
699 observations for quantitative emission estimates and modelling purposes as no uncertainty on the new estimate
700 can be given. Approaches similar to the recent study by ~~Shepherd~~ Shephard et al. (2015b) using an airborne
701 instrument, possibly in combination with an FTIR system focused on the overpass of multiple satellite systems
702 for an extended period of time should be used to establish the sensitivities and biases of the different retrieval
703 products available from satellite instruments as well as the bias between the satellite and surface instruments.
704 The use of IASI and FTIR observations to study NH_3 distributions at ground level requires a combination of
705 model calculations and observations. Such techniques are required to provide all the necessary details to
706 describe the high spatial and temporal variations in NH_3.

707

708 **Acknowledgements**

20

736

21

References

739 Adams, P.J., Seinfeld, J.H., Koch, D., Mickley, L., Jacob, D. (2001), General circulation model assessment of direct radiative forcing by the sulfate-nitrate-ammonium-water inorganic aerosol system, Journal of Geophysical Research Atmospheres, 106 (1), pp. 1097-1111.

743 August, T., Klaes, D., Schlüssel, P., Hultberg, T., Crapeau, M., Arriaga, A., O'Carroll, A., Coppens, D., Munro, R. and Calbet, X.: IASI on Metop-A: Operational Level 2 retrievals after five years in orbit, J. Quant. Spectrosc. Radiat. Transf., 113(11), 1340–1371, doi:10.1016/j.jqsrt.2012.02.028, 2012.

747 Beer, R., Shephard, M. W., Kulawik, S. S., Clough, S. a., Eldering, A., Bowman, K. W., Sander, S. P., Fisher, B. M., Payne, V. H., Luo, M., Osterman, G. B. and Worden, J. R.: First satellite observations of lower tropospheric ammonia and methanol, Geophys. Res. Lett., 35(9), 1–5, doi:10.1029/2008GL033642, 2008.

751 Bleeker, A., Sutton, M. A., Acherman, B., Alebic-Juretic, A., Aneja, V. P., Ellermann, T., Erisman, J. W., Fowler, D., Fagerli, H., Gauger, T., Harlen, K. S., Hole, L. R., Horvath, L., Mitosinkova, M., Smith, R. I., Tang, Y. S., and Pul, A.: Linking ammonia emission trends to measured concentrations and deposition of reduced nitrogen at different scales, in: Atmospheric Ammonia – Detecting emission changes and environmental impacts. Results of an expert workshop under the convention of long-range transboundary air pollution, edited by: Sutton M. A., Reis S., Baker S. M. H. , Atmospheric Ammonia – Detecting emission changes and environmental impacts. Results of an expert workshop under the convention of long-range transboundary air pollution, Springer, 123–180, 2009.

759 Bobbink, R, Hicks K, Galloway J, Spranger T, Alkemade R, Ashmore M, Bustamante M, Cinderby S, Davidson E, Dentener F, Emmett B, Erisman JW, Fenn M, Gilliam F, Nordin A, Pardo L, De Vries W. Global assessment of nitrogen deposition effects on terrestrial plant diversity: a synthesis, Ecological Applications, 20 (2010), pp. 30–59.

764 von Bobrutzki, K., Braban, C. F., Famulari, D., Jones, S. K., Blackall, T., Smith, T. E. L., Blom, M., Coe, H., Gallagher, M., Ghalaieny, M., McGillen, M. R., Percival, C. J., Whitehead, J. D., Ellis, R., Murphy, J., Mohacsi, A., Pogany, A., Junninen, H., Rantanen, S., Sutton, M. A., and Nemitz, E.: Field inter-comparison of eleven atmospheric ammonia measurement techniques, Atmos. Meas. Tech., 3, 91-112, doi:10.5194/amt-3-91-2010, 2010.

769 Brown, L. R., M. R. Gunson, R. A. Toth, F. W. Irion, C. P. Rinsland, and A. Goldman. "1995 atmospheric trace molecule spectroscopy (ATMOS) linelist."*Applied optics* 35, no. 16 (1996): 2828-2848.

771 Chang, L., Palo, S., Hagan, M., Richter, J., Garcia, R., Riggin, D. and Fritts, D.: Structure of the migrating diurnal tide in the Whole Atmosphere Community Climate Model (WACCM), Advances in Space Research, 41(9), 1398–1407, doi:10.1016/j.asr.2007.03.035, 2008.

774 Coheur, P.-F., Clarisse, L., Turquety, S., Hurtmans, D., and Clerbaux, C.: IASI measurements of reactive trace species in biomass burning plumes, Atmos. Chem. Phys., 9, 5655-5667, doi:10.5194/acp-9-5655-2009, 2009.

776 Clarisse, Lieven, Cathy Clerbaux, Frank Dentener, Daniel Hurtmans, and Pierre-François Coheur. "Global ammonia distribution derived from infrared satellite observations." *Nature Geoscience* 2, no. 7 (2009): 479-483.

778 Clarisse, L., Shephard, M. W., Dentener, F., Hurtmans, D., Cady-Pereira, K., Karagulian, F., Van Damme, M., Clerbaux, C. and Coheur, P.-F.: Satellite monitoring of ammonia: A case study of the San Joaquin Valley, J. Geophys. Res., 115(D13), 1–15, doi:10.1029/2009JD013291, 2010.

781 Dammers, E., Vigouroux, C., Palm, M., Mahieu, E., Warneke, T., Smale, D., Langerock, B., Franco, B., Van Damme, M., Schaap, M., Notholt, J., and Erisman, J. W.: Retrieval of ammonia from ground-based FTIR solar spectra, Atmos. Chem. Phys., 15, 12789-12803, doi:10.5194/acp-15-12789-2015, 2015.

784 Dentener, F. J. and Crutzen, P. J.: A three-dimensional model of the global ammonia cycle, J. Atmos. Chem., 19(4), 331–369, doi:10.1007/BF00694492, 1994.

786 Dentener, F., Drevet, J., Lamarque, J. F., Bey, I., Eickhout, B., Fiore, A. M., Hauglustaine, D., Horowitz, L. W., Krol, M., Kulshrestha, U. C., Lawrence, M., Galy-Lacaux, C., Rast, S., Shindell, D., Stevenson, D., Van Noije, T., Atherton, C., Bell, N., Bergman, D., Butler, T., Cofala, J., Collins, B., Doherty, R., Ellingsen, K., Galloway, J., Gauss, M., Montanaro, V., Müller, J. F., Pitari, G., Rodriguez, J., Sanderson, M., Solmon, F., Strahan, S.,

22

Schultz, M., Sudo, K., Szopa, S. and Wild, O.: Nitrogen and sulfur deposition on regional and global scales: A multimodel evaluation, Global Biogeochem. Cycles, 20(4), doi:10.1029/2005GB002672, 2006.

Dils, B., De Mazière, M., Müller, J. F., Blumenstock, T., Buchwitz, M., de Beek, R., Demoulin, P., Duchatelet, P., Fast, H., Frankenberg, C., Gloudemans, A., Griffith, D., Jones, N., Kerzenmacher, T., Kramer, I., Mahieu, E., Mellqvist, J., Mittermeier, R. L., Notholt, J., Rinsland, C. P., Schrijver, H., Smale, D., Strandberg, A., Straume, A. G., Stremme, W., Strong, K., Sussmann, R., Taylor, J., van den Broek, M., Velazco, V., Wagner, T., Warneke, T., Wiacek, A., and Wood, S.: Comparisons between SCIAMACHY and ground-based FTIR data for total columns of CO, CH$_4$, CO$_2$ and N$_2$O, Atmos. Chem. Phys., 6, 1953-1976, doi:10.5194/acp-6-1953-2006, 2006.

EDGAR-Emission Database for Global Atmospheric Research: Source: EC-JRC/PBL. EDGAR version 4.2., http://edgar.jrc.ec.europa.eu, access 15th October 2012, 2011

Erisman, J. W., Hensen, A., Mosquera, J., Sutton, M. and Fowler, D.: Deposition monitoring networks: what monitoring is required to give reasonable estimates of ammonia/ammonium?, Environ. Pollut., 135(3), 419–431, doi:http://dx.doi.org/10.1016/j.envpol.2004.11.015, 2005a.

Erisman, J. W., Vermeulen, A., Hensen, A., Flechard, C., Dämmgen, U., Fowler, D., Sutton, M., Grünhage, L. and Tuovinen, J. P.: Monitoring and modelling of biosphere/atmosphere exchange of gases and aerosols in Europe, Environ. Pollut., 133(3), 403–413, doi:10.1016/j.envpol.2004.07.004, 2005b.

Erisman, J. W., Bleeker, a., Galloway, J. and Sutton, M. S.: Reduced nitrogen in ecology and the environment, Environ. Pollut., 150(1), 140–149, doi:10.1016/j.envpol.2007.06.033, 2007.

Erisman, J. W., Sutton, M. a., Galloway, J., Klimont, Z. and Winiwarter, W.: How a century of ammonia synthesis changed the world, , 1(October 1908), doi:10.1038/ngeo325, 2008.

Erisman, J. W., Galloway, J., Seitzinger, S., Bleeker, A. and Butterbach-Bahl, K.: Reactive nitrogen in the environment and its effect on climate change, Curr. Opin. Environ. Sustain., 3(5), 281–290, doi:10.1016/j.cosust.2011.08.012, 2011.

Farr, T. G., Rosen, P. a., Caro, E. and Crippen, R.: The Shuttle Radar Topography Mission, Rev. …, (2005), 1–33, doi:10.1029/2005RG000183.1.INTRODUCTION, 2007.

Fowler, D., Coyle, M., Skiba, U., Sutton, M. A., Cape, J. N., Reis, S., Sheppard, L. J., Jenkins, A., Grizzetti, B., Galloway, J. N., Vitousek, P., Leach, A., Bouwman, A. F., Butterbach-Bahl, K., Dentener, F., Stevenson, D., Amann, M. and Voss, M.: The global nitrogen cycle in the twenty-first century, Philos. Trans. R. Soc. London B Biol. Sci., 368(1621) [online] Available from: http://rstb.royalsocietypublishing.org/content/368/1621/20130164.abstract, 2013.

Griesfeller, a., Griesfeller, J., Hase, F., Kramer, I., Loës, P., Mikuteit, S., Raffalski, U., Blumenstock, T. and Nakajima, H.: Comparison of ILAS-II and ground-based FTIR measurements of O$_3$, HNO$_3$, N$_2$O, and CH$_4$ over Kiruna, Sweden, J. Geophys. Res., 111(D11), D11S07, doi:10.1029/2005JD006451, 2006.

Hase, F., Blumenstock, T. and Paton-Walsh, C.: Analysis of the instrumental line shape of high-resolution fourier transform IR spectrometers with gas cell measurements and new retrieval software., Appl. Opt., 38(15), 3417–3422, 1999.

Hase, F., Hannigan, J. W., Coffey, M. T., Goldman, a., Höpfner, M., Jones, N. B., Rinsland, C. P. and Wood, S. W.: Intercomparison of retrieval codes used for the analysis of high-resolution, ground-based FTIR measurements, J. Quant. Spectrosc. Radiat. Transf., 87(1), 25–52, doi:10.1016/j.jqsrt.2003.12.008, 2004.

Hase, F., Demoulin, P., Sauval, A. J., Toon, G. C., Bernath, P. F., Goldman, A., Hannigan, J. W., Rinsland, C. P.: An empirical line-by-line model for the infrared solar transmittance spectrum from 700 to 5000 cm(-1), J. Quant. Spectrosc. Ra., 102, 450–463, doi:10.1016/j.jqsrt.2006.02.026, 2006.

Holland, E. a., Dentener, F. J., Braswell, B. H. and Sulzman, J. M.: Contemporary and pre-industrial global reactive nitrogen budgets, Biogeochemistry, 46(1-3), 7–43, doi:10.1007/BF01007572, 1999.

23

Irie, H., Boersma, K. F., Kanaya, Y., Takashima, H., Pan, X. and Wang, Z. F.: Quantitative bias estimates for tropospheric NO2 columns retrieved from SCIAMACHY, OMI, and GOME-2 using a common standard for East Asia, Atmos. Meas. Tech., 5(10), 2403–2411, doi:10.5194/amt-5-2403-2012, 2012.

Kerzenmacher, T., Dils, B., Kumps, N., Blumenstock, T., Clerbaux, C., Coheur, P.-F., Demoulin, P., García, O., George, M., Griffith, D. W. T., Hase, F., Hadji-Lazaro, J., Hurtmans, D., Jones, N., Mahieu, E., Notholt, J., Paton-Walsh, C., Raffalski, U., Ridder, T., Schneider, M., Servais, C., and De Mazière, M.: Validation of IASI FORLI carbon monoxide retrievals using FTIR data from NDACC, Atmos. Meas. Tech., 5, 2751-2761, doi:10.5194/amt-5-2751-2012, 2012.

Leen, J. B., Yu, X. Y., Gupta, M., Baer, D. S., Hubbe, J. M., Kluzek, C. D., Tomlinson, J. M. and Hubbell, M. R.: Fast in situ airborne measurement of ammonia using a mid-infrared off-axis ICOS spectrometer, Environ. Sci. Technol., 47(18), 10446–10453, doi:10.1021/es401134u, 2013.

Luo, M., Shephard, M. W., Cady-Pereira, K. E., Henze, D. K., Zhu, L., Bash, J. O., Pinder, R. W., Capps, S. L., Walker, J. T. and Jones, M. R.: Satellite observations of tropospheric ammonia and carbon monoxide: Global distributions, regional correlations and comparisons to model simulations, Atmos. Environ., 106, 262–277, doi:10.1016/j.atmosenv.2015.02.007, 2015.

Lutsch, E., Dammers, E., Conway, S. and Strong, K: Ground-based FTIR measurements of CO, HCN, C_2H_6 and NH_3 emissions from the 2014 Canadian Wildfires, *in preparation*.

Morgenstern, O., Zeng, G., Wood, S. W., Robinson, J., Smale, D., Paton-Walsh, C., Jones, N. B., and Griffith, D. W. T.: Long-range correlations in Fourier transform infrared, satellite, and modeled CO in the Southern Hemisphere, J. Geophys. Res., 117, D11301 doi:10.1029/2012JD017639, 2012.

Moya, M., Fountoukis, C., Nenes, A., Matías, E., and Grutter, M.: Predicting diurnal variability of fine inorganic aerosols and their gas-phase precursors near downtown Mexico City, Atmos. Chem. Phys. Discuss., 7, 11257-11294, doi:10.5194/acpd-7-11257-2007, 2007.

Nowak, J. B., Neuman, J. A., Kozai, K., Huey, L. G., Tanner, D. J., Holloway, J. S., Ryerson, T. B., Frost, G. J., McKeen, S. A., and Fehsenfeld, F. C.: A chemical ionization mass spectrometry technique for airborne measurements of ammonia, J. Geophys. Res.-Atmos., 112, D10S02, doi:10.1029/2006JD007589, 2007.

Nowak, J. B., Neuman, J. A., Bahreini, R., Brock, C. A., Middlebrook, A. M., Wollny, A. G., Holloway, J. S., Peischl, J., Ryerson, T. B., and Fehsenfeld, F. C.: Airborne observations of ammonia and ammonium nitrate formation over Houston, Texas, J. Geophys. Res.-Atmos., 115, D22 304, doi:10.1029/ 2010JD014195, 2010.

Ohyama, H., Morino, I., Nagahama, T., Machida, T., Suto, H., Oguma, H., Sawa, Y., Matsueda, H., Sugimoto, N., Nakane, H., and Nakagawa, K.: Column-averaged volume mixing ratio of CO2 measured with ground-based Fourier transform spectrometer at Tsukuba, J. Geophys. Res., 114, D18303, doi:10.1029/2008JD011465, 2009.

Paton-Walsh, C., Jones, N. B., Wilson, S. R., Haverd, V., Meier, A., Griffith, D. W. T. and Rinsland, C. P. (2005), Measurements of trace gas emissions from Australian forest fires and correlations with coincident measurements of aerosol optical depth, J. Geophys. Res., 110, D24305, doi:24310.21029/22005JD006202

Pope, III, C. A., Ezzati, M., and Dockery, D. W.: Fine-Particulate Air Pollution and Life Expectancy in the United States, N. Engl. J. Med., 360, 376–386, doi:{10.1056/NEJMsa0805646}, 2009.

Pougatchev, N. S., Connor, B. J., & Rinsland, C. P. (1995). Infrared measurements of the ozone vertical distribution above Kitt Peak. *Journal of Geophysical Research: Atmospheres (1984–2012)*, *100*(D8), 16689-16697.

Puchalski, M. A., M. E. Sather, J. T. Walker, C. M. Lehmann, D. A. Gay, J. Mathew, and W. P. Robarge (2011), Passive ammonia monitoring in the United States: Comparing three different sampling devices, *J. Environ. Monit.*, *13*(11), 3156–3167, doi:10.1039/c1em10553a.

908 Ravishankara, A. R., Daniel, J. S. and Portmann, R. W.: Nitrous oxide (N2O): the dominant ozone-depleting
909 substance emitted in the 21st century., Science, 326(5949), 123–125, doi:10.1126/science.1176985, 2009.
910
911 Rockstrom, J., Steffen, W., Noone, K., Persson, A., Chapin, F. S., Lambin, E. F., Lenton, T. M., Scheffer, M.,
912 Folke, C., Schellnhuber, H. J., Nykvist, B., de Wit, C. A., Hughes, T., van der Leeuw, S., Rodhe, H., Sorlin, S.,
913 Snyder, P. K., Costanza, R., Svedin, U., Falkenmark, M., Karlberg, L., Corell, R. W., Fabry, V. J., Hansen, J.,
914 Walker, B., Liverman, D., Richardson, K., Crutzen, P. and Foley, J. A.: A safe operating space for humanity,
915 Nature, 461(7263), 472–475 [online] Available from: http://dx.doi.org/10.1038/461472a, 2009.
916
917 Rodgers, C. D.: Inverse Methods for Atmospheric Sounding - Theory and Practice, , 2(January), 256,
918 doi:10.1142/9789812813718, 2000.
919
920 Rodgers, C. D. and Connor, B. J.: Intercomparison of remote sounding instruments, J. Geophys. Res. Atmos.,
921 108(D3), n/a–n/a, doi:10.1029/2002JD002299, 2003.
922
923 Rodhe, Henning, Frank Dentener, and Michael Schulz. "The global distribution of acidifying wet
924 deposition." *Environmental Science & Technology* 36.20 (2002): 4382-4388.
925
926 Rothman, L. S., Gordon, I. E., Babikov, Y., Barbe, a., Chris Benner, D., Bernath, P. F., Birk, M., Bizzocchi, L.,
927 Boudon, V., Brown, L. R., Campargue, a., Chance, K., Cohen, E. a., Coudert, L. H., Devi, V. M., Drouin, B. J.,
928 Fayt, a., Flaud, J. M., Gamache, R. R., Harrison, J. J., Hartmann, J. M., Hill, C., Hodges, J. T., Jacquemart, D.,
929 Jolly, a., Lamouroux, J., Le Roy, R. J., Li, G., Long, D. a., Lyulin, O. M., Mackie, C. J., Massie, S. T.,
930 Mikhailenko, S., Müller, H. S. P., Naumenko, O. V., Nikitin, a. V., Orphal, J., Perevalov, V., Perrin, a.,
931 Polovtseva, E. R., Richard, C., Smith, M. a H., Starikova, E., Sung, K., Tashkun, S., Tennyson, J., Toon, G. C.,
932 Tyuterev, V. G. and Wagner, G.: The HITRAN2012 molecular spectroscopic database, J. Quant. Spectrosc.
933 Radiat. Transf., 130, 4–50, doi:10.1016/j.jqsrt.2013.07.002, 2013.
934
935 Schaap, M., van Loon, M., ten Brink, H. M., Dentener, F. J., and Builtjes, P. J. H.: Secondary inorganic aerosol
936 simulations for Europe with special attention to nitrate, Atmos. Chem. Phys., 4, 857-874, doi:10.5194/acp-4-857-
937 2004, 2004
938
939 Schaap, M., Timmermans, R. M. a, Koelemeijer, R. B. a, de Leeuw, G. and Builtjes, P. J. H.: Evaluation of
940 MODIS aerosol optical thickness over Europe using sun photometer observations, Atmos. Environ., 42(9), 2187–
941 2197, doi:10.1016/j.atmosenv.2007.11.044, 2008.
942
943 Senten, C., De Mazière, M., Dils, B., Hermans, C., Kruglanski, M., Neefs, E., Scolas, F., Vandaele, A. C.,
944 Vanhaelewyn, G., Vigouroux, C., Carleer, M., Coheur, P. F., Fally, S., Barret, B., Baray, J. L., Delmas, R., Leveau,
945 J., Metzger, J. M., Mahieu, E., Boone, C., Walker, K. A., Bernath, P. F., and Strong, K.: Technical Note: New
946 ground-based FTIR measurements at Ile de La Réunion: observations, error analysis, and comparisons with
947 independent data, Atmos. Chem. Phys., 8, 3483-3508, doi:10.5194/acp-8-3483-2008, 2008.
948
949 Shephard, M. W., Cady-Pereira, K. E., Luo, M., Henze, D. K., Pinder, R. W., Walker, J. T., Rinsland, C. P.,
950 Bash, J. O., Zhu, L., Payne, V. H., and Clarisse, L.: TES ammonia retrieval strategy and global observations of
951 the spatial and seasonal variability of ammonia, Atmos. Chem. Phys., 11, 10743-10763, doi:10.5194/acp-11-
952 10743-2011, 2011.

953 Shephard, M. W. and Cady-Pereira, K. E.: Cross-track Infrared Sounder (CrIS) satellite observations of
954 tropospheric ammonia, Atmos. Meas. Tech., 8, 1323-1336, doi:10.5194/amt-8-1323-2015, 2015a.

955 Shephard, M. W., McLinden, C. A., Cady-Pereira, K. E., Luo, M., Moussa, S. G., Leithead, A., Liggio, J., Staebler,
956 R. M., Akingunola, A., Makar, P., Lehr, P., Zhang, J., Henze, D. K., Millet, D. B., Bash, J. O., Zhu, L., Wells, K.
957 C., Capps, S. L., Chaliyakunnel, S., Gordon, M., Hayden, K., Brook, J. R., Wolde, M., and Li, S.-M.: Tropospheric
958 Emission Spectrometer (TES) satellite validations of ammonia, methanol, formic acid, and carbon monoxide over
959 the Canadian oil sands, Atmos. Meas. Tech. Discuss., 8, 9503-9563, doi:10.5194/amtd-8-9503-2015, 2015b.

960 Slanina, J., ten Brink, H. M., Otjes, R. P., Even, A., Jongejan, P., Khlystov, A., Waijers-Ijpelaan, A., Hu, M., and
961 Lu, Y.: Continuous analysis of nitrate and ammonium in aerosols by the Steam Jet Aerosol Collector (SJAC),
962 Atmos. Environ., 35, 2319–2330, 2001.

963 Stremme, W., Ortega, I., and Grutter, M.: Using ground-based solar and lunar infrared spectroscopy to study the
964 diurnal trend of carbon monoxide in the Mexico City boundary layer, Atmos. Chem. Phys., 9, 8061-8078,
965 doi:10.5194/acp-9-8061-2009, 2009.

966 Stremme, W., Grutter, M., Rivera, C., Bezanilla, A., Garcia, A. R., Ortega, I., George, M., Clerbaux, C., Coheur,
967 P.-F., Hurtmans, D., Hannigan, J. W., and Coffey, M. T.: Top-down estimation of carbon monoxide emissions
968 from the Mexico Megacity based on FTIR measurements from ground and space, Atmos. Chem. Phys., 13, 1357-
969 1376, doi:10.5194/acp-13-1357-2013, 2013.

970 Sutton, M., Stefan Reis, and Samantha MH Baker. "Atmospheric ammonia." Detecting Emission Changes and
971 Environmental Impacts 494 (2009).

972 Sutton, M. a, Reis, S., Riddick, S. N., Dragosits, U., Nemitz, E., Theobald, M. R., Tang, Y. S., Braban, C. F.,
973 Vieno, M., Dore, A. J., Mitchell, R. F., Wanless, S., Daunt, F., Fowler, D., Blackall, T. D., Milford, C., Flechard,
974 C. R., Loubet, B., Massad, R., Cellier, P., Personne, E., Coheur, P. F., Clarisse, L., Van Damme, M., Ngadi, Y.,
975 Clerbaux, C., Skjøth, C. A., Geels, C., Hertel, O., Wichink Kruit, R. J., Pinder, R. W., Bash, J. O., Walker, J. T.,
976 Simpson, D., Horváth, L., Misselbrook, T. H., Bleeker, A., Dentener, F. and de Vries, W.: Towards a climate-
977 dependent paradigm of ammonia emission and deposition., Philos. Trans. R. Soc. Lond. B. Biol. Sci., 368(1621),
978 20130166, doi:10.1098/rstb.2013.0166, 2013.

979 Sun, K., Cady-Pereira, K., Miller, D. J. , Tao, L., Zondlo, M.A. , Nowak, J. B., Neuman, J. A., Mikoviny, T.,
980 Müller, M. ,Wisthaler, A., Scarino, A. J., and Hostetler, C. A.: Validation of TES ammonia observations at the
981 single pixel scale in theSan Joaquin Valley during DISCOVER-AQ, J. Geophys. Res.-Atmos., 120, 5140–5154,
982 doi:10.1002/2014JD022846, 2015.

984 Toon, G. C., Blavier, J.-F., Sen, B., Margitan, J. J., Webster, C. R., Max, R. D., Fahey, D. W., Gao, R., DelNegro,
985 L., Proffitt, M., Elkins, J., Romashkin, P. A., Hurst, D. F., Oltmans, S., Atlas, E., Schauffler, S., Flocke, F., Bui,
986 T. P., Stimpfle, R. M., Bonne, G. P., Voss, P. B., and Cohen, R. C.: Comparison of MkIV balloon and ER-2
987 aircraft measurements of atmospheric trace gases, J. Geophys. Res., 104, 26 779–26 790, 1999.

989 Van Damme, M., Clarisse, L., Heald, C. L., Hurtmans, D., Ngadi, Y., Clerbaux, C., Dolman, A. J., Erisman, J. W.,
990 and Coheur, P. F.: Global distributions, time series and error characterization of atmospheric ammonia (NH$_3$) from
991 IASI satellite observations, Atmos. Chem. Phys., 14, 2905-2922, doi:10.5194/acp-14-2905-2014, 2014a.

993 Van Damme, M., R. J. Wichink Kruit, M. Schaap, L. Clarisse, C. Clerbaux, P.-F. Coheur, E. Dammers, A. J.
994 Dolman, and J. W. Erisman , Evaluating 4 years of atmospheric ammonia (NH$_3$) over Europe using IASI satellite
995 observations and LOTOS-EUROS model results, J. Geophys. Res. Atmos., 119, 9549–9566,
996 doi:10.1002/2014JD021911, 2014b.

998 Van Damme, M., Clarisse, L., Dammers, E., Liu, X., Nowak, J. B., Clerbaux, C., Flechard, C. R., Galy-Lacaux,
999 C., Xu, W., Neuman, J. a., Tang, Y. S., Sutton, M. a., Erisman, J. W. and Coheur, P. F.: Towards validation of
1000 ammonia (NH$_3$) measurements from the IASI satellite, Atmos. Meas. Tech., 8(3), 1575–1591, doi:10.5194/amt-
1001 8-1575-2015, 2015a.

1003 Van Damme, M., J. W. Erisman, L. Clarisse, E. Dammers, S. Whitburn, C. Clerbaux, A. J. Dolman, and P.-F.
1004 Coheur (2015b), Worldwide spatiotemporal atmospheric ammonia (NH$_3$) columns variability revealed by
1005 satellite, Geophys. Res. Lett., 42, doi:10.1002/2015GL065496.

1007 Velazco, V., Wood, S. W., Sinnhuber, M., Kramer, I., Jones, N. B., Kasai, Y., Notholt, J., Warneke, T.,
1008 Blumenstock, T., Hase, F., Murcray, F. J., and Schrems, O.: Annual variation of strato-mesospheric carbon
1009 monoxide measured by ground-based Fourier transform infrared spectrometry, Atmos. Chem. Phys., 7, 1305-
1010 1312, doi:10.5194/acp-7-1305-2007, 2007.

1012 Vigouroux, C., Hendrick, F., Stavrakou, T., Dils, B., De Smedt, I., Hermans, C., Merlaud, A., Scolas, F., Senten,
1013 C., Vanhaelewyn, G., Fally, S., Carleer, M., Metzger, J.-M., Müller, J.-F., Van Roozendael, M., and De
1014 Mazière, M.: Ground-based FTIR and MAX-DOAS observations of formaldehyde at Réunion Island and
1015 comparisons with satellite and model data, Atmos. Chem. Phys., 9, 9523-9544, doi:10.5194/acp-9-9523-2009,
1016 2009.
1017

1018 Wagner, T., Beirle, S., Grzegorski, M. and Platt, U.: Global trends (1996-2003) of total column precipitable
1019 water observed by Global Ozone Monitoring Experiment (GOME) on ERS-2 and their relation to near-surface
1020 temperature, J. Geophys. Res. Atmos., 111(12), 1–15, doi:10.1029/2005JD006523, 2006.
1021
1022 Whitburn, S., Van Damme, M., Kaiser, J. W., van der Werf, G. R., Turquety, S., Hurtmans, D., Clarisse, L.,
1023 Clerbaux, C. and Coheur, P.-F.: Ammonia emissions in tropical biomass burning regions: Comparison between
1024 satellite-derived emissions and bottom-up fire inventories, Atmos. Environ., 1–13,
1025 doi:10.1016/j.atmosenv.2015.03.015, 2015.
1026
1027 Whitburn, S. Van Damme, M., Clarisse, L., Heald, C., Bauduin, S., Hadji-Lazaro, J., Hurtmans, D., Clerbaux,
1028 C. and Coheur P.-F.:A flexible and robust IASI-NH 3 retrieval algorithm, 2015 (in preparation)
1029
1030 Wiacek, A., Taylor, J. R., Strong, K., Saari, R., Kerzenmacher, T. E., Jones, N. B. and Griffith, D. W. T.:
1031 Ground-Based Solar Absorption FTIR Spectroscopy: Characterization of Retrievals and First Results from a
1032 Novel Optical Design Instrument at a New NDACC Complementary Station, J. Atmos. Ocean. Technol., 24(3),
1033 432–448, doi:10.1175/JTECH1962.1, 2007.
1034
1035 Wood, S. W.: Validation of version 5.20 ILAS HNO 3 , CH 4 , N 2 O, O 3 , and NO 2 using ground-based
1036 measurements at Arrival Heights and Kiruna, J. Geophys. Res., 107(D24), 8208, doi:10.1029/2001JD000581,
1037 2002.
1038
1039 Zhu, L., Henze, D. K., Cady-Pereira, K. E., Shephard, M. W., Luo, M., Pinder, R. W., Bash, J. O. and Jeong, G.
1040 R.: Constraining U.S. ammonia emissions using TES remote sensing observations and the GEOS-Chem adjoint
1041 model, J. Geophys. Res. Atmos., 118(8), 3355–3368, doi:10.1002/jgrd.50166, 2013.
1042

Tables

Table 1 FTIR stations used in the analysis. The location, longitude, latitude and altitude are given for each station as well as the instrument used for the measurements. Typical emission sources are mentioned in the station specifics tab. The topography describesd ~~the typography~~ the geography of the region surrounding the site. N gives the number of observations made during the period of interest. Time period gives the period from which data is used. The last columns describes the used algorithm for the retrieval.

Station Location	Lon	Lat	Altitude (m.a.s.l.)	Instrument	Station specifics	Topography	Time period	N	Retrieval type
Bremen, Germany	8.85E	53.10N	27	Bruker 125 HR	City, fertilizers, livestock	Flat	2008-2015	278	Normal
Toronto, Canada	79.60W	43.66N	174	ABB Bomem DA8	City, fertilizers, biomass burning	On the edge of lake Ontario	2008-2015	1167	Normal
Boulder, United States	105.26W	39.99N	1634	Bruker 120 HR	Fertilizers, biomass burning, livestock	Mountain range to the west	2010-2015	440	Normal
Tsukuba, Japan	140.13E	36.05N	31	Bruker 125 HR	Fertilizers, city	Mostly flat, hills to the north	2014-2015	66	Normal
Pasadena, United States	118.17W	34.20N	460	MKIV_JPL	City, fertilizers, biomass burning	Mountain range to the east	2010-2015	695	Normal
Mexico City, Mexico	99.18W	19.33N	2260	Bruker Vertex 80	City, fires, fertilizers	In between mountain ranges	2012-2015	3980	Normal
St.-Denis, Reunion	55.5E	20.90S	85	Bruker 120 M	Fertilizers, biomass burning, remote	Volcanic	2008-2012	948	Wide
Wollongong, Australia	150.88E	34.41S	30	Bruker 125 HR	Fertilizers, biomass burning, low emissions	Coastal, hills to the west	2008-2015	3641	Wide
Lauder, New Zealand	169.68E	45.04S	370	Bruker 120 HR	Fertilizers, livestock	Hills	2008-2015	1784	Normal

Table 2 Applied data filters to the IASI-NH$_3$ product.

Filter	Filter Criteria
Elevation	|FTIRstation – IASI_Observation| < 300 m
Thermal Contrast	Thermal contrast >12 K
Surface Temperature	T > 275.15 K
IASI-NH$_3$ retrieval Error	None
Cloud cover fraction	<10%
Spatial sampling difference	50 km → 10 km, Δx=5 km
Temporal sampling difference	<90 minutes

Table 3. Summarized results of the comparison between FTIR-NH$_3$ and IASI-NH$_3$ total columns within the coincidence criteria threshold (xdiff < 25 km, tdiff < 90minutes). **N** is the number of averaged total columns, **MRD** is the Mean Relative Difference (in %), **r** and **slope** are the correlation coefficient and slope of the linear regression.

Sites	N	MRD in % (rms 1σ)	r	slope
Bremen	53	-22.5±(54.0)	0.83	0.60
Toronto	170	-46.0±(47.0)	0.79	0.84
Boulder	38	-38.2±(43.5)	0.76	1.11
Tsukuba	15	-28.3±(35.6)	0.67	0.57
Pasadena	16	-47.9±(30.1)	0.59	0.83
Mexico	65	-30.8±(43.9)	0.64	1.14
St.-Denis	20	-61.3±(78.7)	0.65	1.26
Wollongong	62	6.0±(74.3)	0.47	0.92
Lauder	108	-29.7±(57.3)	0.55	0.77
Combined	**547**	**-32.4±(56.3)**	**0.80**	**0.73**

Figures
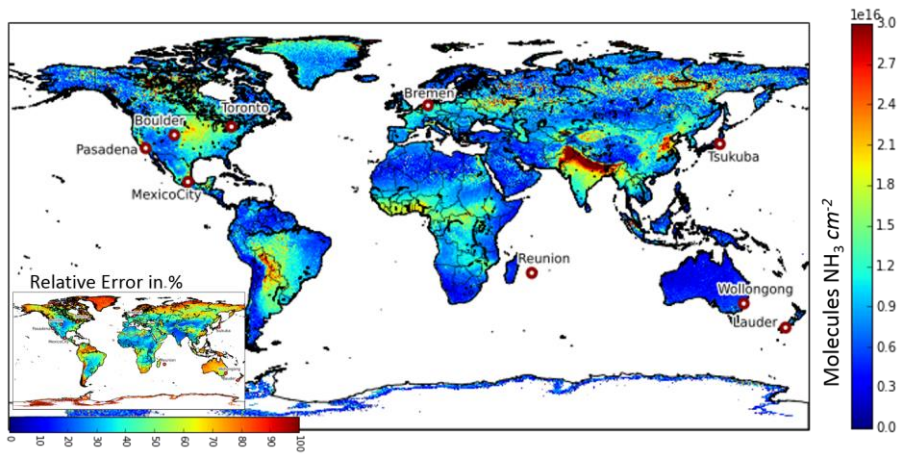
Figure 1. Mean IASI-NH₃ total column distribution for the period between January 2008 and January 2015. The total columns are a weighted average of the individual observations weighted with the relative error. Red circles indicate the positions of the FTIR stations.
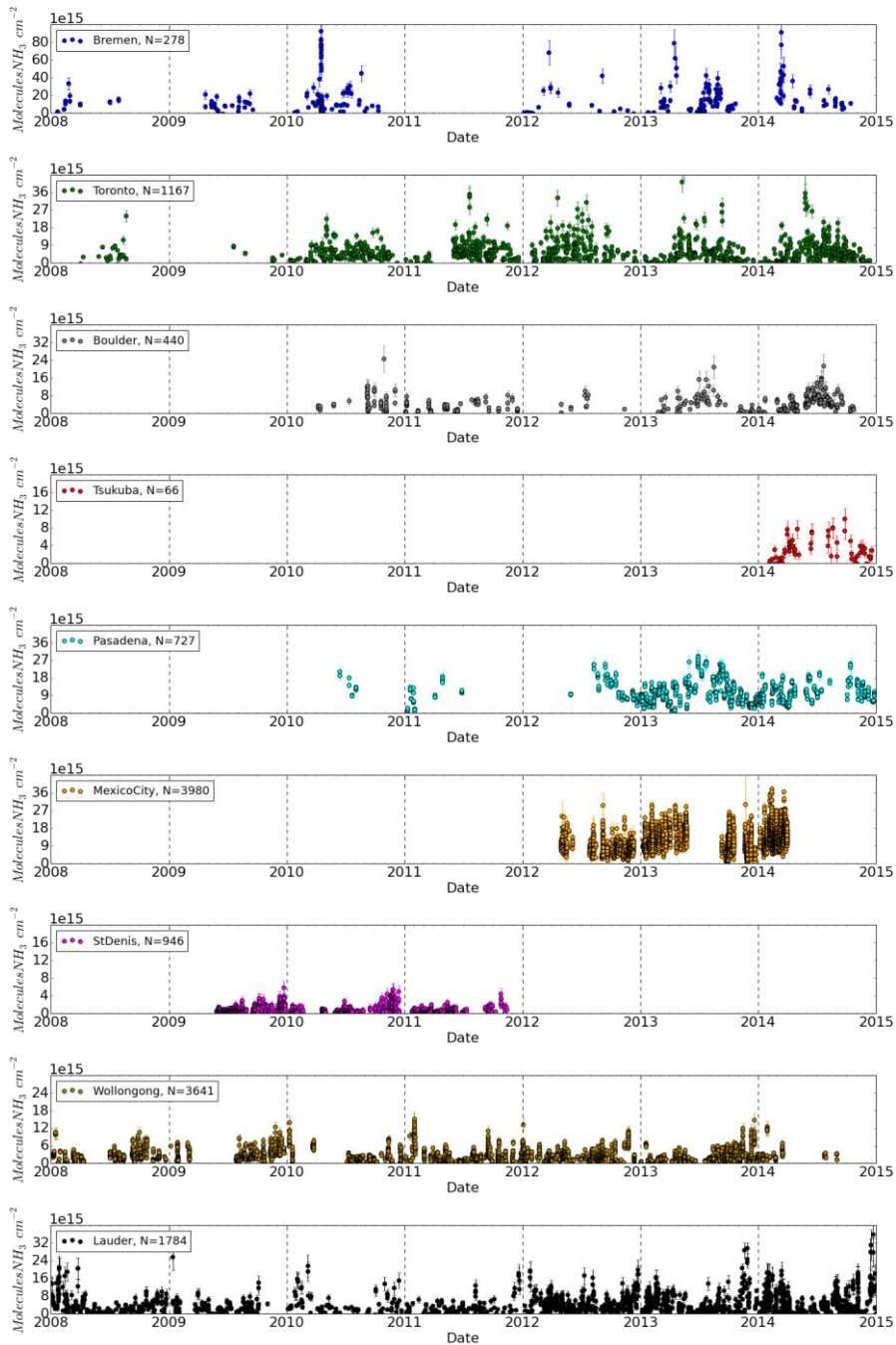
Figure 2. FTIR retrieved NH$_3$ Total Columns (in *molecules cm^{-2}*). Note, the labels on the vertical axis vary for each site.
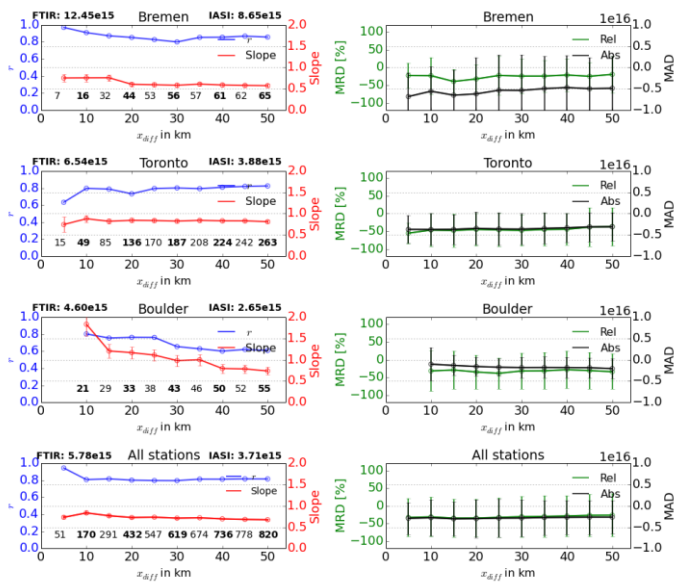
Figure 3. Correlation r (Blue lines, left figures), slope (Red lines, left figures) regression results, Mean Relative Difference (MRD, green lines, right figures) and Mean Absolute Difference (MAD, black lines, right figures) between IASI and FTIR observations as a function of xdiff for a selection of sites. Bars indicate the standard deviation of the slope of the individual regression results. The numbers in the bottom of each subfigure show the number of matching observations. The numbers on the left and right side of the stations name give the mean FTIR and IASI total columns for a xdiff <25 km.
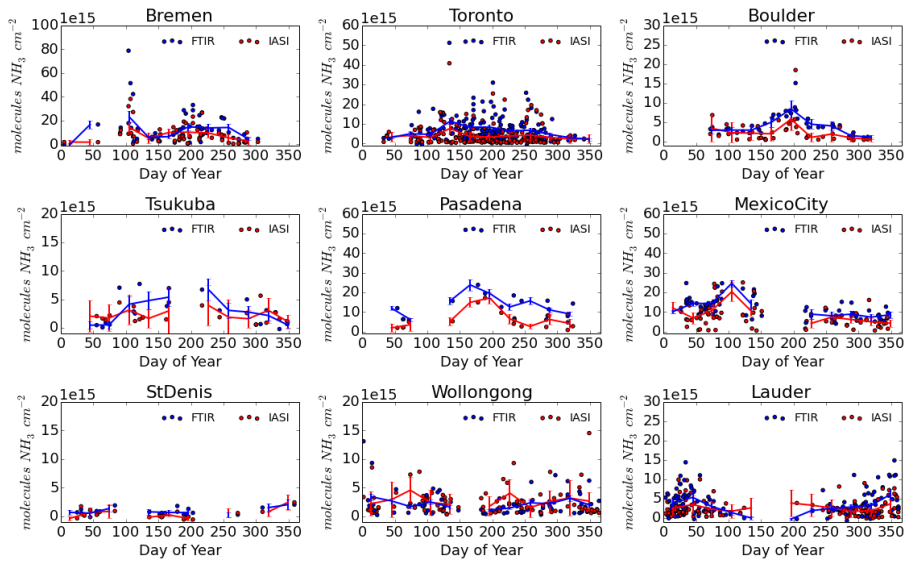
Figure 4. Time series of NH$_3$ for IASI and FTIR datasets with xdiff < 25 km and tdiff < 90minutes (FTIR: Blue and IASI: Red). Scattered values are the observations for each day of year (multiple years of observations). The lines show the monthly mean total columns of the respective sets.
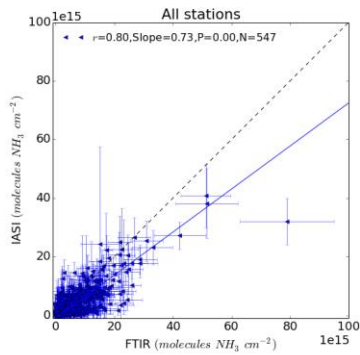

Figure 5. Correlations between the FTIR and IASI total columns with filters thermal contrast > 12K, tdiff < 90min, xdiff < 25 km. The trend line shows the results of the regression analysis.
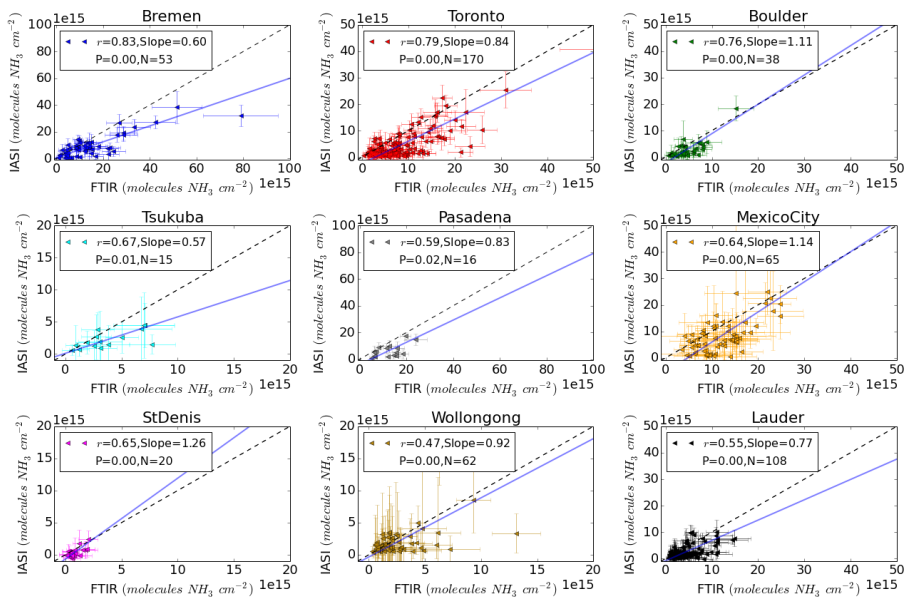
Figure 6. Correlations between the FTIR and IASI total columns with filters thermal contrast > 12, tdiff < 90min, xdiff < 25 km. The trend lines show the results of the regression analysis.
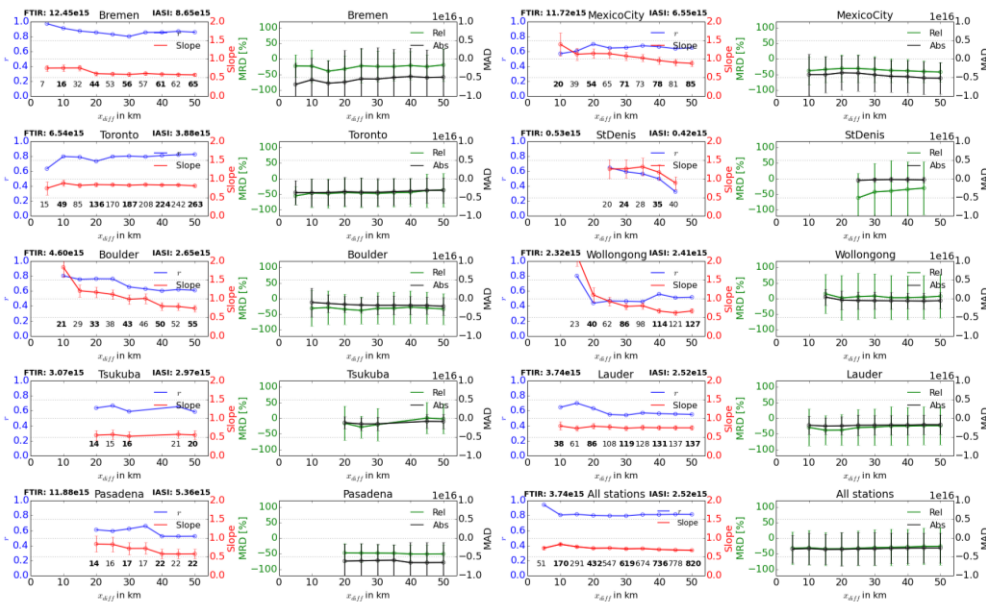
Appendix A

Figure A1. Correlation r (Blue lines, left figures), slope (Red lines, left figures) regression results, Mean Relative Difference (MRD, green lines, right figures) and Mean Absolute Difference (MAD, black lines, right figures) between IASI and FTIR observations as a function of xdiff for all sites. Bars indicate the standard deviation of the slope of the individual regression results. The numbers in the bottom of each subfigure show the number of matching observations. The numbers on the left and right side of the stations name give the mean FTIR and IASI total columns for a xdiff < 25 km.

This section further covers the other stations, in addition to the sites covered by section 3.1.
The results for Mexico City show an overall constant correlation coefficient except for small criteria <20 km. The slope also decreases towards values seen at other stations. This effect could be due to a large number of sources inside the city, i.e. automobile and agricultural emissions in and near the city, increasing the heterogeneity of the found column totals. Reunion and Tsukuba have few coincident observations leading to only a few significant comparisons. This, combined with the low concentrations measured at Reunion leads to large differences in the mean and standard deviations of the subsequent xdiff sets. The Reunion and Wollongong observations are at the sensitivity limit of the IASI-NH$_3$ retrieval which limits the usefulness of the sites for the validation. As there are only a few observations for Tsukuba it is hard to make meaningful conclusions for the variability around the site.